Molecular Modeling of Hydrogen Bonding Fluids: Phase Behavior of Industrial Fluids

Stefan Eckelsbach[1], Martin Bernreuther[2], Cemal Engin[3], Gabriela Guevara-Carrion[3], Yow-Lin Huang[1], Thorsten Merker[3], Hans Hasse[3], and Jadran Vrabec[1]

1 Introduction

The success of process design in chemical engineering and energy technology depends on the availability and accuracy of thermodynamic properties. In recent years, molecular modeling and simulation has become a promising tool to accurately predict thermodynamic properties of fluids. Thermodynamic data can accurately be predicted with molecular models that are based on quantum chemical calculations and are optimized to vapor-liquid equilibrium (VLE) data only.

2 Molecular model class

To describe the intermolecular interactions, a varying number of Lennard-Jones (LJ) sites and superimposed point charges, point dipoles and linear point quadrupoles was used. Point dipoles and quadrupoles were employed for the description of the electrostatic interactions to reduce the computational effort during simulation. However, a point dipole may, e.g. when a simulation program does not support this interaction site type, be approximated by two point charges $\pm q$ separated by a distance l. Analogously, a linear point quadrupole can be approximated by three collinear point charges. A simulation code that does support point dipole and point quadrupole sites is *ms*2 [DES+11].

The parameters of the present molecular models can be separated into three groups. Firstly, the geometric parameters specify the positions of the different in-

[1] Lehrstuhl für Thermodynamik und Energietechnik (ThEt), Universität Paderborn, Warburger Str. 100, 33098 Paderborn · [2] High Performance Computing Center Stuttgart (HLRS), Department Parallel Computing - Training & Application Services, Nobelstr. 19, 70569 Stuttgart · [3] Lehrstuhl für Thermodynamik (LTD), Technische Universität Kaiserslautern, Erwin-Schrödinger-Str. 44, 67663 Kaiserslautern · Author to whom correspondence should be addressed: J. Vrabec. E-mail: jadran.vrabec@upb.de.

teraction sites of the molecular model. Secondly, the electrostatic parameters define the polar interactions in terms of point charges, dipoles and quadrupoles. And finally, the dispersive and repulsive parameters determine the attraction by London forces and the repulsion by overlaps of the electronic orbitals. Here, the LJ-12-6 potential [Jon24a, Jon24b] was used to allow for a straightforward compatibility with the overwhelming majority of the molecular models in the literature.

The total intermolecular interaction energy thus writes as

$$U = \sum_{i=1}^{N-1} \sum_{j=i+1}^{N} \left\{ \sum_{a=1}^{S_i^{\mathrm{LJ}}} \sum_{b=1}^{S_j^{\mathrm{LJ}}} 4\varepsilon_{ijab} \left[\left(\frac{\sigma_{ijab}}{r_{ijab}} \right)^{12} - \left(\frac{\sigma_{ijab}}{r_{ijab}} \right)^{6} \right] + \right.$$

$$\sum_{c=1}^{S_i^{\mathrm{e}}} \sum_{d=1}^{S_j^{\mathrm{e}}} \frac{1}{4\pi\varepsilon_0} \left[\frac{q_{ic} q_{jd}}{r_{ijcd}} + \frac{q_{ic}\mu_{jd} + \mu_{ic} q_{jd}}{r_{ijcd}^2} \cdot f_1(\omega_i, \omega_j) + \frac{q_{ic} Q_{jd} + Q_{ic} q_{jd}}{r_{ijcd}^3} \cdot f_2(\omega_i, \omega_j) + \right.$$

$$\left. \left. \frac{\mu_{ic}\mu_{jd}}{r_{ijcd}^3} \cdot f_3(\omega_i, \omega_j) + \frac{\mu_{ic} Q_{jd} + Q_{ic}\mu_{jd}}{r_{ijcd}^4} \cdot f_4(\omega_i, \omega_j) + \frac{Q_{ic} Q_{jd}}{r_{ijcd}^5} \cdot f_5(\omega_i, \omega_j) \right] \right\}, \quad (1)$$

where r_{ijab}, ε_{ijab}, σ_{ijab} are the distance, the LJ energy parameter and the LJ size parameter, respectively, for the pair-wise interaction between LJ site a on molecule i and LJ site b on molecule j. The permittivity of vacuum is ε_0, whereas q_{ic}, μ_{ic} and Q_{ic} denote the point charge magnitude, the dipole moment and the quadrupole moment of the electrostatic interaction site c on molecule i and so forth. The expressions $f_x(\omega_i, \omega_j)$ stand for the dependency of the electrostatic interactions on the orientations ω_i and ω_j of the molecules i and j [AT87, GG84]. Finally, the summation limits N, S_x^{LJ} and S_x^{e} denote the number of molecules, the number of LJ sites and the number of electrostatic sites of molecule x, respectively.

For a given molecule, i.e. in a pure fluid throughout, the interactions between LJ sites of different type were defined by applying the standard Lorentz-Berthelot combining rules [Lor81, Ber98]

$$\sigma_{ijab} = \frac{\sigma_{iiaa} + \sigma_{jjbb}}{2}, \quad (2)$$

and

$$\varepsilon_{ijab} = \sqrt{\varepsilon_{iiaa}\varepsilon_{jjbb}}. \quad (3)$$

3 Molecular properties from quantum chemistry

Molecular models that were developed on the basis of quantum chemical (QC) calculations stand between *ab initio* models and empirical models. The present strategy is based on the idea to include *ab initio* information without giving up the freedom to reasonably optimize the model to important macroscopic thermodynamic properties. Thus, for the modeling process some experimental data are needed for optimization. The chosen properties, vapor pressure and saturated liquid density, have

the advantage to be well available for numerous engineering fluids and to represent dominant features of the fluid state.

3.1 Geometry

All geometric data of the molecular models, i.e. bond lengths, bond angles and dihedrals, were specified on the basis of QC calculations. Therefore, a geometry optimization, i.e. an energy minimization, was initially performed using GAMESS(US) [SBB+93]. The Hartree-Fock level of theory was applied with a relatively small (6-31G) basis set.

The resulting configuration of the atoms was taken to specify the spatial distribution of the LJ sites, except for the sites that represent groups containing Hydrogen atoms. As the united atom approach was used to obtain computationally efficient molecular models, the dispersive and repulsive interactions of the Hydrogen atoms were modeled together with the atom they are bonded to. For the Methyl (CH_3) united atom site, the LJ potential was located at the geometric mean of the nuclei, while the Methine (CH) united atom site was located at 0.4 of the distance between Carbon and Hydrogen atom. These empirical offsets are in good agreement with the results of Ungerer *et al.* [UBD+00], which were found by optimization of transferable molecular models for n-Alkanes.

3.2 Electrostatics

Intermolecular electrostatic interactions mainly occur due to static polarities of single molecules that can well be obtained by QC. Here, the Møller-Plesset 2 level of theory was used that considers electron correlation in combination with the polarizable 6-311G(d,p) basis set.

The purpose of the present work was the development of effective pair potentials with state-independent model parameters. Obviously, the electrostatic interactions are stronger in the liquid state than in the gaseous state due to the higher density. Furthermore, the mutual polarization raises their magnitude in the liquid. Thus, for the calculation of the electrostatic moments by QC a liquid-like state should be considered. This was done here by placing one molecule into a dielectric continuum and assigning the experimental dielectric constant of the liquid to it, as in the COSMO method.

From the resulting electron density distribution for the small symmetric molecules studied here, the dipole and quadrupole moments were estimated by simple integration over the orbitals. Thus magnitudes and orientations of these electrostatic interaction sites were derived from QC calculations.

3.3 Dispersion and repulsion

It would be highly desirable to also calculate the dispersive and repulsive interactions using *ab initio* methods as well. This approach was followed by different authors in the past, predominantly for simple molecules. However, from an engineering point of view, this leads to difficulties.

For an estimation of dispersive and repulsive interactions at least two molecules must be taken into account. To properly scan the energy hyper surface, many QC calculations for different distances and orientations of the molecules have to be performed. As the dispersive, and partly also the repulsive, interactions are usually only a very small fraction of the total energy calculated by QC, highly accurate methods like coupled cluster (CC) with large basis sets or even extrapolations to the basis set limit must be used for this task [SC07].

Due to the fact that this is computationally too expensive for engineering purposes, LJ parameters for a given atom or molecular group were passed on from other molecular models. Some of these parameters were subsequently fitted in the optimization process to yield an accurate VLE behavior of the modeled pure substance.

4 Pure fluid models

None of the six molecules developed in the present work (Hydrogen chloride, Phosgene, Toluene, Benzene, Chlorobenzene and Ortho-Dichlorobenzene) exhibits significant conformational changes. Their internal degrees of freedom were thus neglected and the molecular models were chosen to be rigid, using the most stable configuration as determined by QC.

The optimization was performed using a Newton scheme following Stoll [Sto05, EVH08a]. The applied method has many similarities with the one published by Bourasseau *et al.* [BHB+03]. It relies on a least-square minimization of a weighted fitness function that quantifies the deviations of simulation results for a given molecular model compared to reference data.

Correlations for vapor pressure, saturated liquid density and enthalpy of vaporization, taken from the DIPPR database [RWO+06], were used as reference data for model adjustment and evaluation. This was done even in cases where the correlations are based only on few true experimental data points, as they were regarded as best practice. The quantitative comparison between simulation results and correlations of experimental data was done by applying fits to the simulation data according to Lotfi *et al.* [LVF92]. The relative deviation between fit and correlation was calculated in steps of 1 K in the temperature range where simulations were performed and is denoted by "mean unsigned error" in the following.

VLE were simulated with the Grand Equilibrium method [VH02] that is implemented in the *ms*2 simulation code [DES+11]. The optimized parameter sets of the new molecular models are given in [HHHV11].

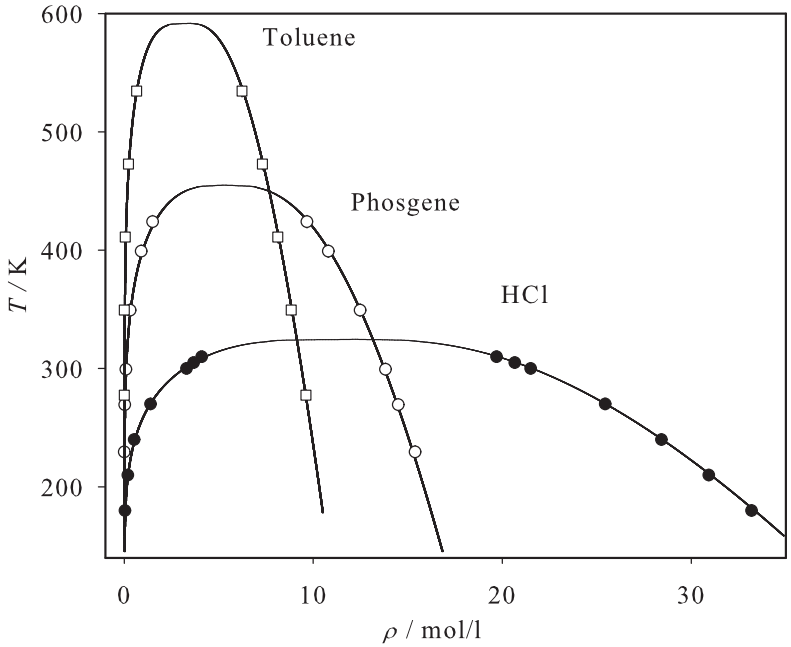

Fig. 1 Saturated densities; present simulation data: ● Hydrogen chloride, ○ Phosgene, □ Toluene; correlations of experimental data [RWO+06]: —.

The pure substance VLE simulation results on the basis of these optimized models are shown in absolute terms in Figures 1 to 3, where they are compared to the DIPPR correlations of experimental data.

Figure 2 illustrates the influence of molecular size and polarity on the phase envelope in a systematic manner. Both size and polarity increase in the sequence Benzene, Chlorobenzene, Ortho-Dichlorobenzene which is reflected by a decreasing average saturated liquid density and an increasing critical temperature.

The critical properties were determined through fits to the present VLE simulation results as suggested by Lotfi *et al.* [LVF92]. The estimated uncertainties of critical temperature, critical density and critical pressure from simulation are 1, 3 and 3 %, respectively. Table 1 compares these critical properties to experimental data [Mat72, Amb80, AT95, AKZ68, BR70]. An excellent agreement was achieved, being almost throughout within the combined error bars.

For Hydrogen chloride, Phosgene and Benzene experimental data on the second virial coefficient are available [DT77, NS81, Tso78, PPM92]. Figure 4 compares the predictions based on the present molecular models with these data. The agreement is very good, only at low temperatures noticeable deviations are present for the smaller two molecules.

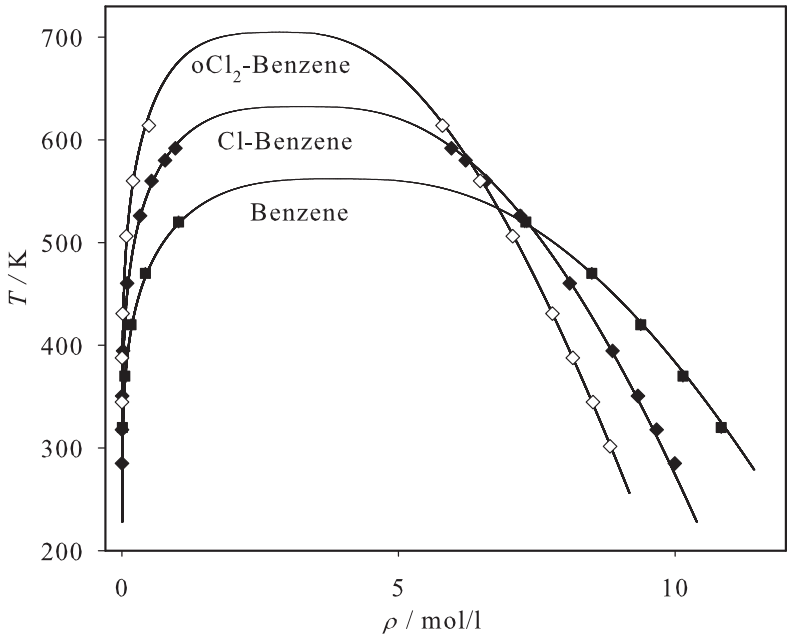

Fig. 2 Saturated densities; present simulation data: ■ Benzene, ♦ Chlorobenzene, ◇ Ortho-Dichlorobenzene; correlations of experimental data [RWO+06]: —.

Table 1 Critical properties of the pure substances on the basis of the new molecular models in comparison to recommended experimental data. The number in parentheses indicates the experimental uncertainty in the last digit.

	T_c^{sim} K	T_c^{exp} K	ρ_c^{sim} mol/l	ρ_c^{exp} mol/l	p_c^{sim} MPa	p_c^{exp} MPa	Ref.
Hydrogen chloride	324	324.65 (5)	12.2	12.34 (3)	8.3	8.31 (5)	[Mat72]
Phosgene	454	455.0 (7)	5.1	5.40 (6)	5.7	5.35 (4)	[Amb80]
Benzene	563	562.15 (6)	3.9	3.88 (2)	4.9	4.9 (1)	[AT95]
Chlorobenzene	631	632.35 (8)	3.2	3.24 (7)	4.6	4.52 (8)	[AKZ68]
Ortho-Dichlorobenzene	705	705.0 (9)	2.8	2.77 (6)	4.0	4.1 (3)	[BR70]
Toluene	592	591.75 (8)	3.4	3.20 (4)	4.1	4.08 (3)	[AT95]

5 Influence of the intramolecular degrees of freedom on vapor-liquid equilibrium of ammonia

The influence of the intramolecular interactions on the VLE was investigated, taking ammonia as a case study.

The introduction of the intramolecular interactions on the basis of the harmonic potentials with the force constants by Shi and Maginn [SM09] into the originally rigid model by Eckl *et al.* [EVH08b] has a strong influence on the VLE properties. On average, the vapor pressure is decreased by 38 %, the saturated liquid den-

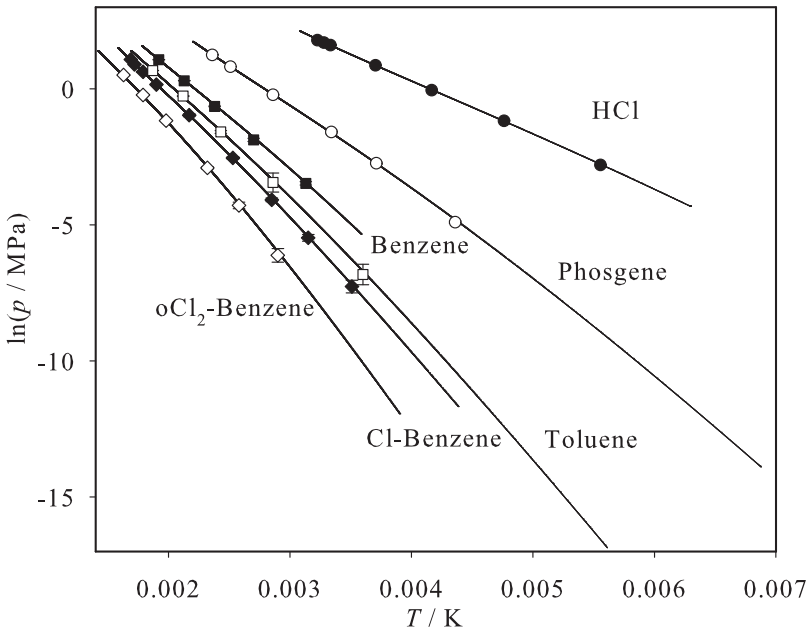

Fig. 3 Vapor pressure; present simulation data: ● Hydrogen chloride, ○ Phosgene, ■ Benzene, □ Toluene ♦ Chlorobenzene, ◇ Ortho-Dichlorobenzene; correlations of experimental data [RWO+06]: —.

sity is increased by 11 % and the enthalpy of vaporization is increased by 31 % [EMHV11]. As usual, the saturated vapor density follows the trend of the vapor pressure.

The reasons for these discrepancies were studied in detail using the VLE at 347.5 K as an example. The observed major shift of VLE properties are the result of the significant change in the molecular geometry of the flexible molecule in the liquid phase. Due to the intermolecular interactions the flexible molecules oscillate in the liquid state around an average bond angle of 103.2°, instead of 106° in case of the equilibrium structure, which was adopted for the rigid model. The three partial dipoles, each constituted by the Nitrogen atom and one Hydrogen atom, are thus more aligned so that the overall dipole moment distribution has an average value of $\bar{\mu}^{liq} = 2.06$ D. This dipole moment distribution is 10 % higher than the equilibrium value of $\mu = 1.88$ D, cf. Figure 5 (top). In the vapor state, the dipole moment distribution exhibits an average value of $\bar{\mu}^{vap} = 1.92$ D, which is only negligibly higher than that of the equilibrium structure, cf. Figure 5 (bottom). This shows that as expected, for the studied conditions, the molecules in the vapor state oscillate around a geometry that is only marginally different from the equilibrium structure.

In summary: the strong intermolecular interactions in the liquid state lead to changes of the flexible molecular model's structure that significantly influence the

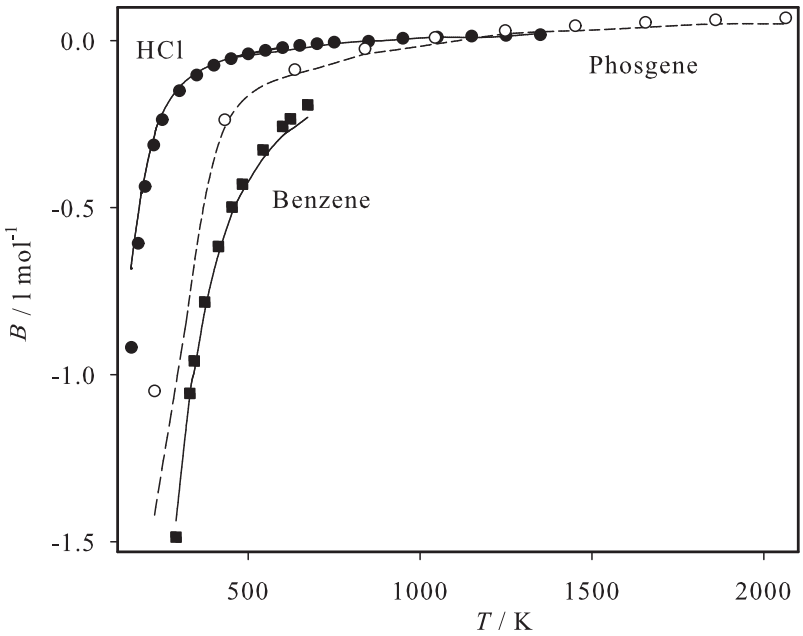

Fig. 4 Second virial coefficient; present simulation data: ● Hydrogen chloride, ○ Phosgene, ■ Benzene; correlations of experimental data [DT77, NS81, Tso78, PPM92]: —, - -.

thermodynamic properties, whereas in the vapor state, only minor changes are observed.

Table 2 Influence of the intramolecular degrees of freedom on the vapor-liquid equilibrium of ammonia at 347.5 K for different models with constant intermolecular interaction potential parameters. In the *rigid* model, both the bond length and the bond angle were kept fixed. In the *bond length* model, the bond angle was fixed, whereas the bond length was allowed to vary. In the *bond angle* model, the bond length was fixed, whereas the bond angle was allowed to vary. In the *flexible* model, both the bond length and the bond angle were allowed to vary. The force constants by Shi and Maginn [SM09] were used in those cases where the intramolecular degrees of freedom were introduced. "Exp." denotes reference data from the NIST Chemistry Webbook [NIST10].

Model	ρ^{liq} mol/l	ρ^{vap} mol/l	p MPa	Δh_v kJ/mol	$\bar{\mu}^{liq}$ D	$\bar{\mu}^{vap}$ D
rigid	30.3 (1)	1.73 (3)	3.69 (7)	15.9 (4)	1.88	1.88
bond length	30.5 (1)	1.69 (3)	3.67 (5)	16.1 (4)	1.88	1.88
bond angle	33.0 (2)	1.05 (8)	2.5 (1)	19.3 (5)	2.05	1.89
flexible	33.3 (2)	0.98 (5)	2.36 (5)	19.6 (6)	2.06	1.92
Exp.	30.4	1.73	3.66	15.5		1.47

The influence of the different intramolecular degrees of freedom types on the VLE properties was also studied at the temperature 347.5 K. In the *rigid* model,

both the bond length and the bond angle were kept fixed. In the *bond length* model, the bond angle was fixed, whereas the bond length was allowed to vary. In the *bond angle* model, the bond length was fixed, whereas the bond angle was allowed to vary. In the *flexible* model, both the bond length and the bond angle were allowed to vary. It can be seen in Table 2 that the bond angle potential is crucial, whereas the bond length potential has hardly any effect on the VLE properties of ammonia.

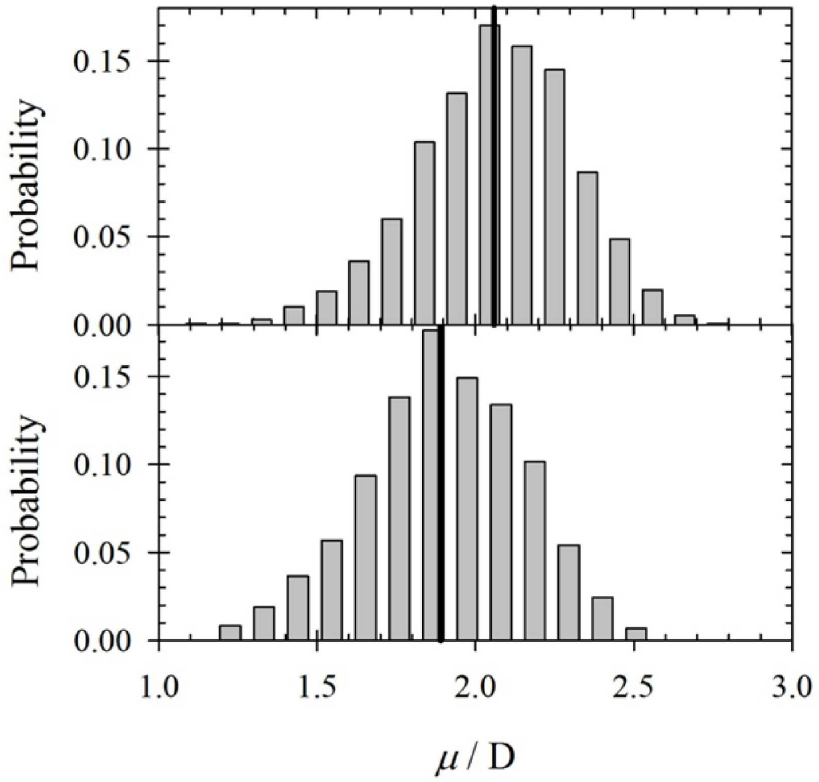

Fig. 5 Distribution of the dipole moment magnitude in the saturated liquid (top) and saturated vapor (bottom) at 347.5 K of the rigid ammonia model [EVH08b] with superimposed intramolecular degrees of freedom, using the force constants by Shi and Maginn [SM09]. The data were sampled from six uncorrelated configurations. The vertical lines indicate the average molecular dipole moments $\bar{\mu}^{liq} = 2.06$ D and $\bar{\mu}^{vap} = 1.92$ D in the coexisting phases.

The observed changes of the VLE properties can be explained by the increase of the attractive molecular interactions due to the increased average dipole moment in the liquid state. The average potential energy between two dipoles [Pra69] is

$$u_{\mu\mu} = -\frac{2}{3}\frac{\mu_i^2\mu_j^2}{k_B T r^6}, \tag{4}$$

which indicates that the dipole-dipole potential energy depends on the fourth power of the dipole moment. The dipole-dipole interaction yields on average an attractive contribution so that a relative increase of $\Delta\mu/\mu_0$ of the dipole moment leads to a relative increase of the total potential energy of $\Delta u_{\mu\mu}/u^0_{\mu\mu} \geq 4\Delta\mu/\mu_0$. The charge distribution of ammonia has a quadrupole moment as well, however, the dipole moment is dominant. There is also an additional cooperative effect resulting from the configuration of the molecules, because intramolecular degrees of freedom enhance the ability of the molecules to avoid highly repulsive configurations.

6 Compiler performance building executables of the molecular simulation code ms2

Most of the simulation data presented in this work were generated with the molecular simulation code *ms*2 [DES+11] that is developed in our group.

It was extensively tested on different platforms regarding different aspects like parallelization or vectorization. In this work, the compiler performance executables of *ms*2 is highlighted for molecular dynamics (MD) and Monte Carlo (MC) simulations.

Throughout, the equimolar liquid mixture of methanol and ethanol at 298.15 K and 0.1 MPa was simulated in the *NpT* ensemble [GNVH08]. Methanol was modeled by two LJ sites and three point charges and ethanol by three LJ sites and three point charges [SSVH07]. This test case was chosen, because it is a typical application. Similar results are expected for a wide class of problems. However, note that the actual run times will differ with varying thermodynamic conditions that are simulated. Run times increase with higher density of the system, among others.

*ms*2 is distributed as a source code and can be compiled with a wide variety of compilers. However, the performance is significantly influenced by the compiler and the linker as well as by the used options. Figure 6 shows the runtime of the test case on different platforms using different compilers. The binaries were generated by

- GNU gfortran* with "-fdefault-real-8 -O3"
- Intel ifortran† with "-r8 -fast"
- PGI pgf95‡ with "-r8 -fastsse"
- Sun Studio sunf90§ with "-r8const -fast"
- Pathscale pathf90¶ with "-r8 -Ofast"

with options activated to enforce the use of double precision floating point numbers. The chosen optimization flags represent a common choice.

* http://gcc.gnu.org/fortran/

† http://software.intel.com/en-us/intel-compilers/

‡ http://www.pgroup.com/products/

§ http://developers.sun.com/sunstudio/

¶ http://www.pathscale.com/

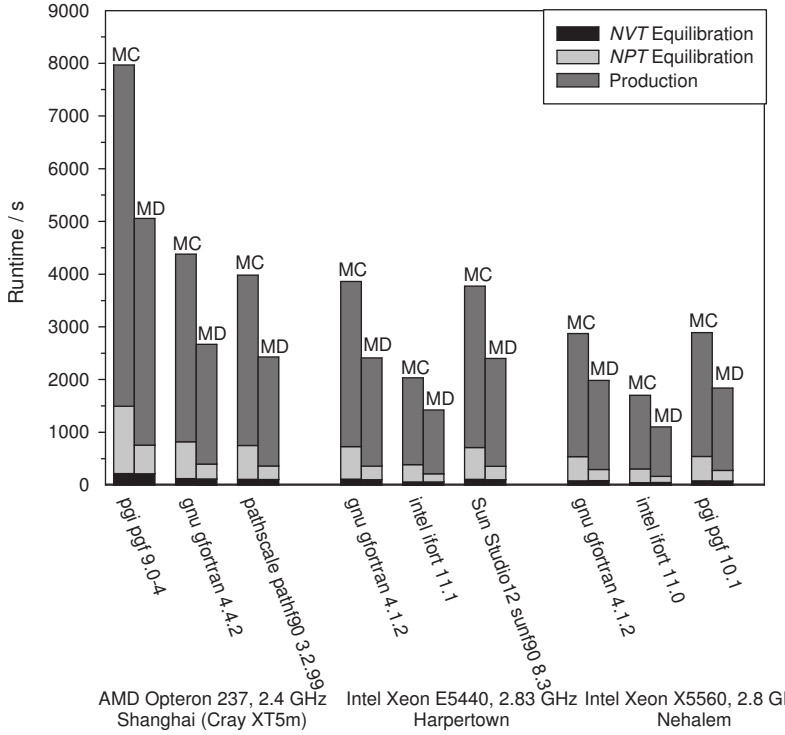

Fig. 6 Runtime of the testcase executed by *ms*2 as measured on different platforms using different compilers. An equimolar liquid mixture of methanol and ethanol at 298.15 K and 0.1 MPa was simulated in the *NpT* ensemble.

The best combination of compiler and platform was the Intel ifortran compiler and the Intel Xeon X5560 "Nehalem" processor[‖]. An Intel ifortran compiled binary of *ms*2 significantly outperforms binaries compiled by GNU gfortran and PGI pgf90, independent of the computing platform.

7 Conclusion

Six rigid molecular models were proposed for Hydrogen chloride, Phosgene, Toluene, Benzene, Chlorobenzene and Ortho-Dichlorobenzene. The interaction sites were located according to the atom positions resulting from *ab initio* quantum chemical calculations. Also the electrostatic interactions were parameterized according to high-level *ab initio* quantum chemical results. The latter were obtained by calculations within a dielectric continuum to mimic the (stronger) interactions in the liquid

[‖] `http://www.hlrs.de/systems/platforms/nec-nehalem-cluster/`

state. The LJ parameters were adjusted to VLE data, namely vapor pressure and saturated liquid density.

Even for very small molecules like ammonia, the introduction of intramolecular degrees of freedom may have an astonishingly large influence on VLE properties. Thus, care has to be taken upon combining force field parameterizations covering different aspects of the molecular interactions.

8 Acknowledgements

We gratefully acknowledge support by Deutsche Forschungsgemeinschaft. This work was carried out under the auspices of the Boltzmann-Zuse Society (BZS) of Computational Molecular Engineering. The simulations were performed on the NEC SX-9 and the NEC Nehalem Cluster at the High Performance Computing Center Stuttgart (HLRS).

References

[AKZ68] Alani, G. H.; Kudchadker, A. P.; Zwolinski, B. J. *Chem. Rev.* **1968,** *68*, 659.
[Amb80] Ambrose, D. *Vapor-liquid critical properties;* National Physical Laboratory Report Chem 107, Middlesex, 1980.
[AT87] Allen, M. P.; Tildesley D. J. *Computer Simulations of Liquids;* Oxford University Press: Oxford, 1987.
[AT95] Ambrose, D.; Tsonopoulos, C. *J. Chem. Eng. Data* **1995,** *40*, 547.
[Ber98] Berthelot, D. *Cr. Hebd. Acad. Sci.* **1898,** *126*, 1703.
[BHB+03] Bourasseau, E.; Haboudou, M.; Boutin, A.; Fuchs, A. H.; Ungerer, P. *J. Chem. Phys.* **2003,** *118*, 3020.
[BR70] Bunger, W. B.; Riddick, J. A. *Organic Solvents: Physical Properties and Methods of Purification;* 3rd ed., Wiley Online Library: New York, 1970.
[DES+11] Deublein, S.; Eckl, B.; Stoll, J.; Lishchuk, S.; Guevara-Carrion, G.; Glass, C. W.; Merker, T.; Bernreuther, M.; Hasse, H.; Vrabec, J. *Comput. Phys. Commun.* **2011,** in press, doi:10.1016/j.cpc.2011.04.026, `http://www.ms-2.de/`.
[DT77] Danner, R. P.; Tarakad, R. R. *AIChE J.* **1977,** *23*, 685.
[EMHV11] Engin, C.; Merker, T.; Hasse, H.; Vrabec, J. *Mol. Phys.* **2011,** *109*, 619.
[EVH08a] Eckl, B.; Vrabec, J.; Hasse, H.; *J. Phys. Chem. B* **2008,** *112*, 12710.
[EVH08b] Eckl, B.; Vrabec, J.; Hasse, H. *Mol. Phys.* **2008,** *106*, 1039.
[GG84] Gray, C. G.; Gubbins, K. E. *Theory of Molecular Fluids. 1. Fundamentals;* Clarendon Press: Oxford, 1984.
[GNVH08] Guevara-Carrion, G.; Nieto-Draghi, C.; Vrabec, J.; Hasse, H. *J. Phys. Chem. B* **2008,** *112*, 16664.
[HHHV11] Huang, Y.-L.; Heilig, M.; Hasse, H.; Vrabec, J. *AIChE J.* **2011,** *57*, 1043.
[Jon24a] Jones, J. E. *Proc. R. Soc. A* **1924,** *106*, 441.
[Jon24b] Jones, J. E. *Proc. R. Soc. A* **1924,** *106*, 463.
[Lor81] Lorentz, H. A. *Ann. Phys.* **1881,** *12*, 127.
[LVF92] Lotfi, A.; Vrabec, J.; Fischer, J. *Mol. Phys.* **1992,** *76*, 1319.
[Mat72] Mathews, J. F. *Chem. Rev.* **1972,** *72*, 71.
[NIST10] National Institute of Standards and Technology *NIST Chemistry Webbook 2010;* `http://webbook.nist.gov/`.

[NS81] Nunes Da Ponte, M.; Staveley, L. A. K. *J. Chem. Thermodyn.* **1981,** *13*, 179.
[PPM92] Polt, A.; Platzer, B.; Maurer, G. *Chem. Tech. Leipzig* **1992,** *44*, 216.
[Pra69] Prausnitz, J. M. *Molecular Thermodynamics of Fluid-Phase Equilibria;* Prentice-Hall, Inc., Englewood Cliffs: New Jersey, 1969.
[RWO+06] Rowley, R. L.; Wilding, W. V.; Oscarson, J. L.; Yang, Y.; Zundel, N. A.; Daubert, T. E.; Danner, R. P. *DIPPR Data Compilation of Pure Compound Properties. Design Institute for Physical Properties;* AIChE: New York, 2006.
[SBB+93] Schmidt, M. W.; Baldridge, K. K.; Boatz, J. A.; Elbert, S. T.; Gordon, M. S.; Jensen, J. H.; Koseki, S.; Matsunaga, N.; Nguyen, K. A.; Shujun, S.; Windus, T. L.; Dupuis, M.; Montgomery, A. M. *J. Comput. Chem* **1993,** *14*, 1347.
[SC07] Sandler, S. I.; Castier, M. *Pure. Appl. Chem.* **2007,** *79*, 1345.
[SM09] Shi, W.; Maginn, E. J. *AIChE J.* **2009,** *55*, 2414.
[SSVH07] Schnabel, T.; Srivastava, A.; Vrabec, J.; Hasse, H. *J. Phys. Chem. B* **2007,** *111*, 9871.
[Sto05] Stoll, J. *Molecular Models for the Prediction of Thermophysical Properties of Pure Fluids and Mixtures;* Fortschritt-Berichte VDI, Reihe 3, Vol. 836, VDI-Verlag: Düsseldorf, 2005.
[Tso78] Tsonopoulos, C. *AIChE J.* **1978,** *24*, 1112.
[UBD+00] Ungerer, P.; Beauvais, C.; Delhommelle, J.; Boutin, A.; Rousseau, B.; Fuchs, A. H. *J. Chem. Phys.* **2000,** *112*, 5499.
[VH02] Vrabec, J.; Hasse, H. *Mol. Phys.* **2002,** *100*, 3375.